

## Tuning exchange bias in Ni/FeF<sub>2</sub> heterostructures using antidot arrays

M. Kovylna,<sup>1,a)</sup> M. Erekhinsky,<sup>2</sup> R. Morales,<sup>3</sup> J. E. Villegas,<sup>4</sup> I. K. Schuller,<sup>2</sup> A. Labarta,<sup>1</sup> and X. Batlle<sup>1,b)</sup>

<sup>1</sup>Departament de Física Fonamental and Institut de Nanociència i Nanotecnologia, Universitat de Barcelona, Barcelona, 08028 Catalonia, Spain

<sup>2</sup>Department of Physics, University of California San Diego, La Jolla, California 92093, USA

<sup>3</sup>Departamento de Física, Universidad de Oviedo-CINN, Oviedo 33007, Spain

<sup>4</sup>Unité Mixte de Physique CNRS/Thales, Université Paris Sud, 91405 Orsay, France

(Received 6 August 2009; accepted 24 September 2009; published online 14 October 2009)

The transition from positive to negative exchange bias can be systematically tuned with antidot arrays artificially introduced into Ni/FeF<sub>2</sub> ferromagnetic/antiferromagnetic heterostructures. These results are a consequence of the energy balance and suggest that the nanostructure plays a key role in the formation of pinned uncompensated spin regions in the antiferromagnetic FeF<sub>2</sub> layer. These noninterfacial magnetic moments created at the antidot faces favor the onset of positive exchange bias at lower cooling fields. © 2009 American Institute of Physics. [doi:10.1063/1.3248306]

The comprehensive explanation of exchange bias (EB) in ferromagnetic (FM)/antiferromagnetic (AF) heterostructures and nanostructures still remains a challenge, despite the extensive experimental and theoretical investigations.<sup>1–5</sup> EB is usually described as an additional unidirectional anisotropy induced by the AF into the FM via exchange coupling at the interface. Recently, negative EB (NEB) and positive EB (PEB),<sup>6</sup> i.e., hysteresis loops shifted either against or along the cooling field direction, have been reported.<sup>7–10</sup> The occurrence of PEB seems to be critically related to the interplay among the AF coupling at the FM/AF interface, domain wall (DW) energies in both the FM and AF, and the Zeeman energy between the cooling field ( $H_{FC}$ ) and interface spins. Moreover, when the “EB domain,” i.e., the area for which the pinned uncompensated interfacial AF spins induce the same unidirectional anisotropy, is comparable to or larger than the FM domain size, each FM domain couples mostly to one EB domain.<sup>7,8</sup> Consequently, for small/large  $H_{FC}$  only one EB direction arises (NEB/PEB), while two directions appear for intermediate  $H_{FC}$ , resulting in a bidomain state leading to double hysteresis loops (DHLs).<sup>7,8</sup> Much work has been performed in FM/FeF<sub>2</sub> heterostructures since FeF<sub>2</sub> is an AF (Néel temperature  $T_N=78.4$  K) that may be grown epitaxially, leading to thin films with large crystallographic domains. However, the origin of the pinned spins giving raise to PEB remains uncertain.

The relevant length scales in EB have been studied largely on nanostructured samples,<sup>4,5</sup> in particular, on FM/AF nanodots and FM nanodots deposited onto continuous AF layers.<sup>5,11</sup> Nevertheless, there are only few reports investigating EB in ordered arrays of antidots,<sup>12–14</sup> with distances and/or sizes comparable to FM and/or AF domain lengths. In these, the effect of lateral confinement on EB and magnetization reversal mechanisms can be probed. While either an enhancement<sup>12,14</sup> or a decrease<sup>13</sup> of the EB field compared to continuous films was found, contradictory results have also been found regarding the asymmetry of the hysteresis loops.<sup>12</sup> Enhancement of EB field in AF/FM heterostructures with patterned FM layer was explained by the suppres-

sion of FM-FM exchange interactions in the FM domains.<sup>14</sup> In addition the effect of nanostructuring on the PEB onset has not been reported so far.

In this letter, ordered antidot arrays have been patterned by focused ion beam (FIB) lithography into Ni/FeF<sub>2</sub> heterostructures. We find that the PEB onset can be controlled with the antidot density (AD), although the EB field remains almost unaltered after patterning. As a consequence the  $H_{FC}$  at which the PEB onset appears, decreases with increasing AD. This unexpected behavior is explained in terms of the formation of pinned uncompensated AF spins at the antidot faces below the  $T_N$ . These spins increase the Zeeman energy of AF domains, favoring the alignment with the  $H_{FC}$  and the occurrence of PEB.

Ni/FeF<sub>2</sub> heterostructures were deposited by electron beam evaporation onto (110) MgF<sub>2</sub> single-crystal substrates of 70 nm of FeF<sub>2</sub> at 300 °C, 50 nm of Ni, and 4 nm of Al (to prevent oxidation) at 150 °C. The films were deposited at a rate of 1 Å/s. X-ray diffraction showed that FeF<sub>2</sub> grew epitaxial and untwined in the (110) orientation. Based on the bulk structure, the ideal (110) FeF<sub>2</sub> plane is assumed to have compensated spins, oriented in-plane and with the easy axis along the [001] direction of the crystal structure [Fig. 1(d)]. Magnetization measurements showed that the polycrystalline Ni layer displayed a growth-induced uniaxial anisotropy along the FeF<sub>2</sub> easy axis, as expected.<sup>7,15</sup> In order to obtain a variety of identical samples, the layers were deposited onto a 1 cm<sup>2</sup> (110) MgF<sub>2</sub> substrate patterned by photolithography in the form of seven stripes 10 μm wide and 90 μm long, and with all the electrodes required to measure the four probe magnetotransport in an external magnetic field,  $H$  [Fig. 1(c)]. The long side of the stripes [given by the  $I^+ - I^-$  direction in Fig. 1(c)] was chosen parallel to the FeF<sub>2</sub> [001] easy axis (and consequently, to the Ni one). Square arrays of 200 nm square antidots were patterned by FIB lithography through the whole depth of the heterostructure [Figs. 1(a) and 1(b)]. The antidots were carved in square shapes with in-plane sides parallel and perpendicular to the [001] FeF<sub>2</sub> crystal direction [Fig. 1(d)]. Magnetoresistance (MR) curves were measured before nanopatterning and only those samples with less than a 4% deviation in the MR loops were FIB patterned (ion beam current of 30 pA). The antidot squareness and depth profile were *in situ* characterized during the etching

<sup>a)</sup>Electronic mail: miroslavna@ffn.ub.es.

<sup>b)</sup>Electronic mail: xavierbatlle@ub.edu.

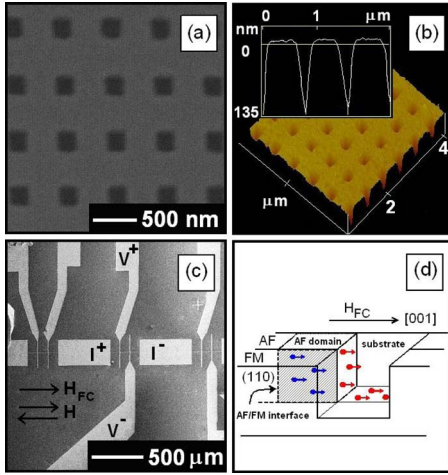


FIG. 1. (Color online) (a) SEM image for the AD=0.12. (b) Atomic force microscopy image for AD=0.12. The inset shows that the antidot is carved through the whole depth of the heterostructure. (c) Electrode configuration for MR measurements. (d) Schematic of net AF magnetic moments in FeF<sub>2</sub> antidots yielding PEB. Black (blue) arrows represent pinned uncompensated interfacial spins (in contact with the FM) while gray (red) arrows symbolize pinned uncompensated spins created at the antidot faces (not in contact with the FM).

process by scanning ion/scanning electron microscopy (SEM) and *ex situ* by atomic force microscopy [Figs. 1(a) and 1(b)]. The nominal AD was obtained as the ratio between the area of the patterned region and the total area of the sample.

MR measurements were carried out after field cooling the samples from 150 K—well above the FeF<sub>2</sub>  $T_N=78.4$  K—down to 4.2 K at a field  $H_{FC}$  applied parallel to the easy axis of the AF [Figs. 1(c) and 1(d)]. The resistance of the stripes was obtained by measuring the constant current (2 mA) voltage drop, in an  $H$  parallel to the stripes and dc current (parallel geometry). Additional measurements with both in-plane  $H_{FC}$  and  $H$  perpendicular to the stripes (transversal geometry; not shown) confirmed that the easy axis of FeF<sub>2</sub> was along the [001] direction, both before and after the FIB patterning.

MR is well suited to study the EB in the present nanostructures. First, it allows measuring a small patterned area, it is very sensitive to local magnetization and provides the loop asymmetry which is related to the reversal mode. Second, and most important, it is determined only by the FM Ni through which the current flows, since FeF<sub>2</sub> is an insulator. Therefore, the anisotropic MR of the Ni layer with the parallel current-to-field geometry is essentially proportional to  $M_{\perp}^2/M^2$ , where  $M_{\perp}$  is the transverse component of the magnetization and  $M$  is the total magnetization. For all samples, the antidot side-to-side distance is much larger than the typical Ni DW width (tens of nanometers)<sup>8,17</sup> and of the order of the EB domains (larger than hundreds of nanometers),<sup>7,11</sup> so it is reasonable to assume that the patterning does not affect the relevant length scales of the system.

Figure 2 shows the MR, defined as  $[R(H)-R_{sat}]/R_{sat}$ , with  $R(H)$  and  $R_{sat}$  the resistances at a field  $H$  and at the largest applied field, respectively. These are shown for  $H_{FC}=0.19, 0.4, 2.5, 5,$  and  $20$  kOe, and for three representative antidot arrays with AD=0.07, 0.12, and 0.24, corresponding to side-to-side distances of  $683 \pm 12, 373 \pm 10,$  and  $207 \pm 12$  nm, respectively. Both the decreasing and increasing field branches are shown in Fig. 2. MR peaks develop in

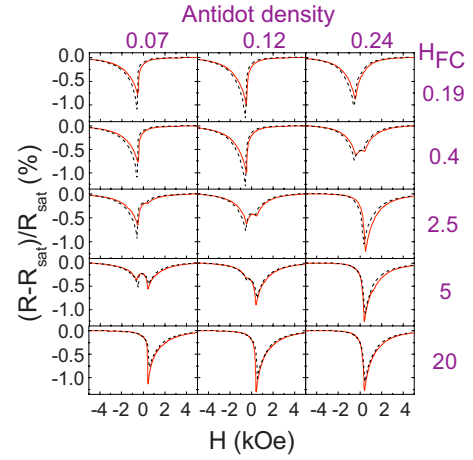


FIG. 2. (Color online)  $[R(H)-R_{sat}]/R_{sat}$  measured at 4.2 K as a function of  $H$  applied parallel to the current, after cooling under  $H_{FC}=0.19, 0.4, 2.5, 5,$  and  $20$  kOe, for AD=0.07, 0.12, and 0.24. The solid (red)/dash (black) line corresponds to the decreasing/increasing field branches.

both field branches around the  $H$  at which the major part of the magnetization reversal takes place: for small  $H_{FC}$ , the MR peaks are shifted toward negative fields (NEB), while for large  $H_{FC}$ , the shifts are PEB. For  $H_{FC} < 0.4$  kOe, all samples show NEB, while for  $H_{FC} > 20$  kOe, all samples display PEB. For intermediate  $H_{FC}$ , two MR peaks are observed in each field branch, one shifted to NEB, the other to positive fields (PEB), with relative height and areas dependant on  $H_{FC}$  and AD (Fig. 2).

For NEB, the field-decreasing branch of MR shows an abrupt, irreversible downturn, probably associated with an in-plane DW nucleation and propagation.<sup>9,16,17</sup> As negative saturation is approached this is followed by a much smoother, reversible increase, probably related to the (incoherent) rotation associated with the winding of an incomplete DW in the FM.<sup>9,16,17</sup> For PEB, the MR curves proceed through the same reversal mechanisms following the increasing-field branch of the MR—instead of the decreasing one—as positive saturation is approached, as expected.<sup>9,16,17</sup> The existence of this *reflection* symmetry between NEB and PEB in the magnetization reversal process is evident by comparing in Fig. 2 the shape of the decreasing field branch of the MR curve at  $H_{FC}=0.19$  kOe (NEB) to the increasing branch at  $H_{FC}=20$  kOe (PEB), for AD  $\leq 0.12$ . Except for minor differences, NEB and PEB peaks are essentially identical mirror images.

An estimate of the EB field,  $H_{EB}$ , may be obtained from the peak positions in the MR curves.<sup>18</sup>  $H_{EB}$  shows a slight dependence on  $H_{FC}$ , for all samples including the unpatterned samples with AD=0 (not shown). While at  $H_{FC}=0.19$  kOe and 20 kOe  $|H_{EB}|$  displays a smooth decreasing trend with increasing AD (see Table I), the values for  $H_{EB}$  for intermediate  $H_{FC}$  (i.e., when DHL appear) are within the same range (not shown).

TABLE I. Negative ( $H_{NEB}$ )/positive ( $H_{PEB}$ ) EB fields obtained from the peak positions in the MR curves at  $T=4$  K and after cooling the samples under 0.19/20 kOe, as a function of the AD.

AD	0	0.07	0.12	0.24
$H_{NEB}$ (Oe)	$-557 \pm 50$	$-533 \pm 40$	$-525 \pm 30$	$-465 \pm 40$
$H_{PEB}$ (Oe)	$523 \pm 9$	$516 \pm 7$	$498 \pm 8$	$467 \pm 7$

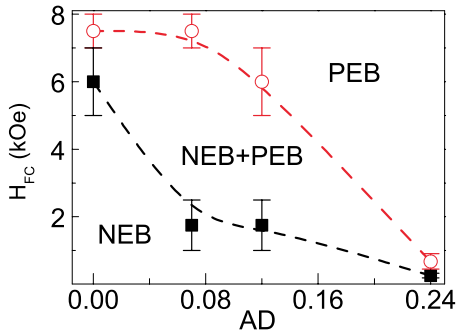


FIG. 3. (Color online) Cooling fields,  $H_{FC}$ , corresponding to the onset of PEB (solid squares) and to those at which NEB disappears (empty circles), as functions of the AD. Dashed lines are guides to the eyes showing the region where the bidomain state takes place.

In contrast, the AD has a very large effect on the  $H_{FC}$  for which the onset of PEB occurs (solid squares in Fig. 3) and the field at which NEB disappears (empty circles in Fig. 3). For example, PEB appears at  $H_{FC}$  one order of magnitude smaller for  $AD=0.24$  than for the unpatterned film, suggesting that the antidot patterning produces additional pinned uncompensated AF spins. In addition, the  $H_{FC}$  range for which the bidomain state takes place first increases with AD until about  $AD=0.07$  and then rapidly shrinks as  $AD=0.24$  is approached (Fig. 3). This indicates that the antidot carving strongly enhances the existence of regions within the AF that favor the onset of PEB.

All the results imply therefore that in the patterned samples, the EB domains are larger than or comparable to the FM domains, such that local, nonaveraging EB is observed.<sup>7,8</sup> At intermediate  $H_{FC}$ , the samples split into two magnetic subsystems that behave independently of each other, giving rise to peak shifts in the MR of almost the same magnitude but opposite sign. Therefore, while for small or large  $H_{FC}$  the FM domains couple to one EB direction, leading to single hysteresis loops with either NEB or PEB, FM domains may couple to two EB directions for intermediate  $H_{FC}$ , leading to DHL.

Finally, the origin of the effect of AD on the onset of PEB may be understood from the nanostructure of the patterned samples. The antidot carving may produce regions of locally pinned uncompensated spins throughout the antidot faces of the  $FeF_2$ . Figure 1(d) illustrates two types of uncompensated AF magnetic moments. Black (blue) arrows represent pinned uncompensated interfacial AF moments, which determine the EB magnitude. Grey (red) arrows indicate pinned uncompensated moments at the antidot faces created by FIB patterning. These magnetic moments possibly are responsible for the Zeeman energy increase, which reduces the  $H_{FC}$  necessary for the onset of PEB. PEB appears in unpatterned films as the Zeeman term  $E_Z^{\text{film}} = c_Z n_{AF/FM} a_{AF/FM} H_{FC}$  overcomes the exchange coupling energy at the interface  $E_I^{\text{film}} = c_I n_{AF/FM} a_{AF/FM} - c_Z$  and  $c_I$  are proportionality constants,  $n_{AF/FM}$  is the areal density of net pinned uncompensated AF magnetic moments at the AF/FM interface, and  $a_{AF/FM}$  is the contact area between AF and FM layers. In case of patterned antidots the contact area is smaller,  $a'_{AF/FM}$ , the interfacial energy has the same form,  $E_I^{\text{pattern}} = c_I n_{AF/FM} a'_{AF/FM}$  but there is an extra term in the Zeeman energy,  $E_Z^{\text{pattern}} = c_Z n_{AF/FM} a'_{AF/FM} H_{FC} + c_Z n_{\text{antidot}} a_{\text{antidot}} H_{FC}$ , where  $a_{\text{antidot}}$  and  $n_{\text{antidot}}$  are the area of the antidot faces and the areal density of net pinned uncompensated AF magnetic

moments created in those faces, respectively. Both “black (blue)” and “grey (red)” magnetic moments [see Fig. 1(d)] align with the cooling field simultaneously since they belong to the same AF domain and become pinned below  $T_N$ , in agreement with the domain state model.<sup>3,19</sup> Thus the grey (red) spins in the antidot faces lead to a reduction of the  $H_{FC}$  necessary to overcome the exchange coupling  $E_I^{\text{pattern}}$  as compared to the continuous film. Moreover, higher ADs increase the face area  $a_{\text{antidot}}$  leading to a monotonous decrease of the onset of PEB as observed in Fig. 3. This result demonstrates that the appearance of PEB can be tuned by the AD, generating noninterfacial magnetic moments in AF domains.

In conclusion, PEB and NEB have been shown in square arrays of 200 nm Ni/ $FeF_2$  antidots. Single and double MR loops with similar values of  $|H_{EB}|$  can be tuned by the cooling protocol. Cooling fields one order of magnitude smaller as compared to those for the unpatterned film are required to obtain PEB for the largest AD studied. This result is qualitatively explained by taking into account the Zeeman and exchange energy balance. Uncompensated spin regions in the antidot faces contribute to the Zeeman energy but not to the exchange coupling, reducing the minimum  $H_{FC}$  necessary for the appearance of PEB. Consequently, we have shown that the onset of PEB in EB antidots can be controlled by the AD density.

The financial support of the Spanish MEC (Project Nos. MAT2006-03999 and MAT2009-08667, and Ph.D. grant of M.K.), Catalan DURSI (Grant No. 2009SGR856) and the U.S. Air Force Office for Scientific Research are recognized. R.M. also acknowledges funding from the Marie Curie OIF.

- <sup>1</sup>J. Nogués and I. K. Schuller, *J. Magn. Magn. Mater.* **192**, 203 (1999).
- <sup>2</sup>M. Kiwi, *J. Magn. Magn. Mater.* **234**, 584 (2001).
- <sup>3</sup>U. Nowak, K. D. Usadel, J. Keller, P. Miltényi, B. Beschoten, and G. Güntherodt, *Phys. Rev. B* **66**, 014430 (2002).
- <sup>4</sup>J. Nogués, J. Sort, V. Langlais, V. Skumryev, S. Suriñach, J. S. Muñoz, and M. D. Baró, *Phys. Rep.* **422**, 65 (2005).
- <sup>5</sup>O. Iglesias, A. Labarta, and X. Batlle, *J. Nanosci. Nanotechnol.* **8**, 2761 (2008).
- <sup>6</sup>J. Nogués, D. Lederman, T. J. Moran, and I. K. Schuller, *Phys. Rev. Lett.* **76**, 4624 (1996).
- <sup>7</sup>I. V. Roshchin, O. Petravic, R. Morales, Z.-P. Li, X. Batlle, and I. K. Schuller, *Europhys. Lett.* **71**, 297 (2005).
- <sup>8</sup>O. Petravic, Z.-P. Li, I. V. Roshchin, M. Viret, R. Morales, X. Batlle, and I. K. Schuller, *Appl. Phys. Lett.* **87**, 222509 (2005).
- <sup>9</sup>M. R. Fitzsimmons, D. Lederman, M. Cheon, H. Shi, J. Olamit, I. V. Roshin, and I. K. Schuller, *Phys. Rev. B* **77**, 224406 (2008).
- <sup>10</sup>M. R. Fitzsimmons, B. J. Kirby, S. Roy, Z.-P. Li, I. V. Roshchin, S. K. Sinha, and I. K. Schuller, *Phys. Rev. B* **75**, 214412 (2007).
- <sup>11</sup>Z.-P. Li, R. Morales, and I. K. Schuller, *Appl. Phys. Lett.* **94**, 142503 (2009).
- <sup>12</sup>D. Tripathy, A. O. Adeyeye, and N. Singh, *Appl. Phys. Lett.* **93**, 022502 (2008); D. Tripathy and A. O. Adeyeye, *Phys. Rev. B* **79**, 064413 (2009).
- <sup>13</sup>C. Jiang, D. Xue, X. Fan, D. Guo, and Q. Liu, *Nanotechnology* **18**, 335703 (2007).
- <sup>14</sup>K. Liu, S. M. Baker, M. Tuominen, T. P. Russell, and I. K. Schuller, *Phys. Rev. B* **63**, 060403 (2001).
- <sup>15</sup>J. Nogués, T. J. Moran, D. Lederman, I. K. Schuller, and K. V. Rao, *Phys. Rev. B* **59**, 6984 (1999).
- <sup>16</sup>Z.-P. Li, O. Petravic, R. Morales, J. Olamit, X. Batlle, K. Liu, and I. K. Schuller, *Phys. Rev. Lett.* **96**, 217205 (2006).
- <sup>17</sup>R. Morales, Z.-P. Li, O. Petravic, X. Batlle, and I. K. Schuller, *Appl. Phys. Lett.* **89**, 072504 (2006).
- <sup>18</sup>T. Gredig, I. N. Krivorotov, P. Eames, and E. D. Dahlberg, *Appl. Phys. Lett.* **81**, 1270 (2002).
- <sup>19</sup>P. Miltényi, M. Gierlings, J. Keller, B. Beschoten, G. Güntherodt, U. Nowak, and K. D. Usadel, *Phys. Rev. Lett.* **84**, 4224 (2000).